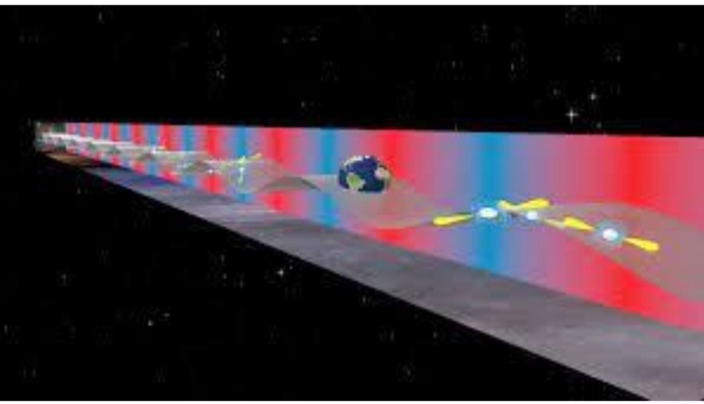

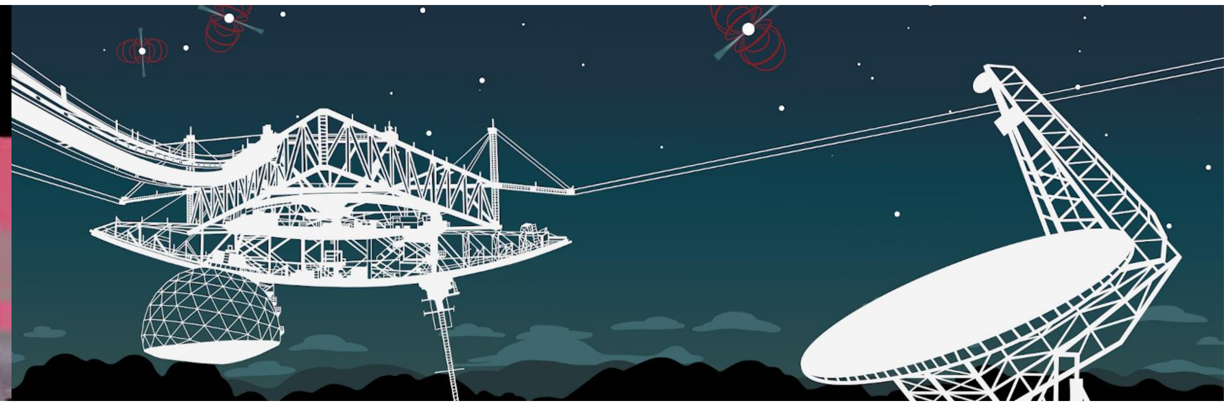

Gravitational Waves from Early-Universe Turbulence:

Can we observe the QCD phase transition-generated gravitational waves through pulsar timing arrays?

Tina Kahniashvili

Carnegie Mellon University, USA & Ilia State University, Georgia

In collaboration with:
Axel Brandenburg, Emma Clarke, Yutong He

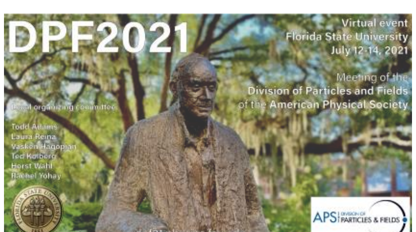

Based on: arXiv: 2102.12428

DPF21, July 14, 2021

Outline

- ✓ Gravitational waves from primordial turbulence
- ✓ Numerical simulations
- ✓ NANOGrav signal possible sources:
  - QCD energy scales
- ✓ What is next?

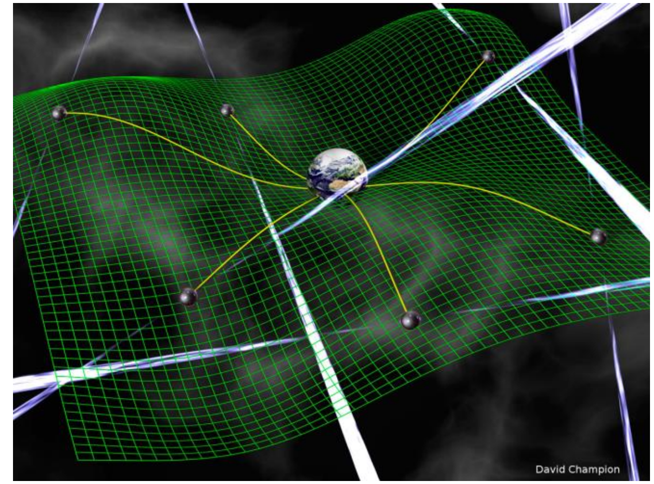

Connection with High Energy Particle Physics – the best laboratory to test the energy scales EVEN near the Planck scale

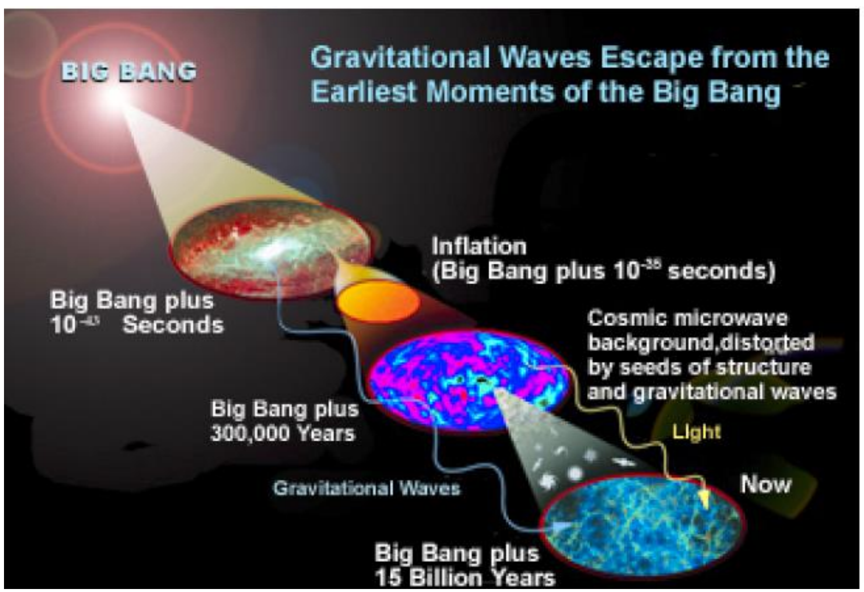

- The very early universe (inflation)
- Topological defects/strings
- Cosmological phase transitions
  - Bubble nucleation/collisions
  - Sound waves
  - Hydro turbulence
  - MHD turbulence

gravitational waves from anisotropic stresses

Mon. Not. R. astr. Soc. (1987) **229**, 357–370

$$\nabla^2 h_{ij}(\boldsymbol{x},t) - \frac{\partial^2}{\partial t^2} h_{ij}(\boldsymbol{x},t) = -16\pi G\, S_{ij}(\boldsymbol{x},t)$$

Generation of gravitational waves by the anisotropic phases in the early Universe

Magnetic fields;
Turbulence (hydro & MHD)

D. V. Deryagin, D. Yu. Grigoriev and V. A. Rubakov *Institute for Nuclear Research, USSR Academy of Sciences, Moscow 117312, USSR*

M. V. Sazhin *P. K. Sternberg Astronomical Institute, Universitetskii pr. 13, Moscow 119899, USSR*

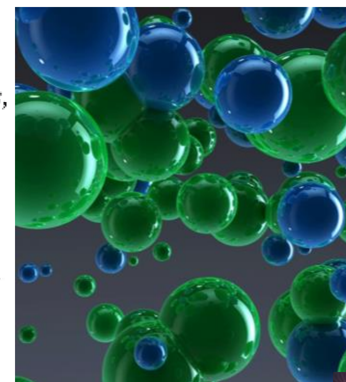

The space interferometer will be a unique device to observe the gravitational radiation from anisotropic phases possible at the energy scales T=1TeV-100GeV.

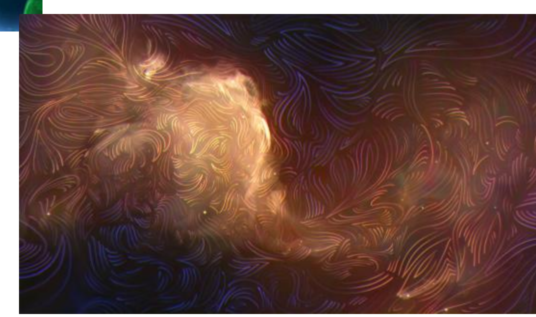

Pulsar Timing Array (PTA) are sensible to gravitational waves generated or present at QCD energy scales

gravitational waves from phase transitions

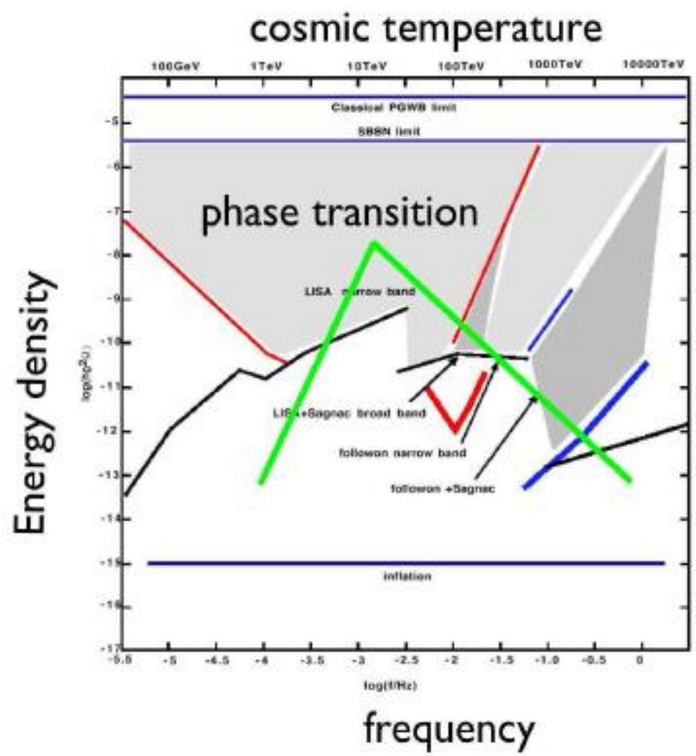

C. Hogan, 2006

Pioneering works:

- Winicour 1973
- Hogan 1982, 1986
- Turner & Wilczek 1990
- Kosowsky, Turner, Watkins. 1992
- Kosowsky & Turner 1993
- Kamionkowski et al. 1994

VOLUME 69, NUMBER 14 PHYSICAL REVIEW LETTERS 5 OCTOBER

Gravitational Waves from First-Order Cosmological Phase Transitions

Arthur Kosowsky,[1,2] Michael S. Turner,[1,2,3] and Richard Watkins[1,3]
[1]*NASA/Fermilab Astrophysics Center, Fermi National Accelerator Laboratory, Batavia, Illinois 60510-0500*
[2]*Department of Physics, Enrico Fermi Institute, The University of Chicago, Chicago, Illinois 60637-1433*
[3]*Department of Astronomy & Astrophysics, Enrico Fermi Institute, The University of Chicago, Chicago, Illinois 60637-*
(Received 6 December 1991; revised manuscript received 26 May 1992)

A first-order cosmological phase transition that proceeds through the nucleation and collision of true-vacuum bubbles is a potent source of gravitational radiation. Possibilities for such include first-order inflation, grand-unified-theory-symmetry breaking, and electroweak-symmetry breaking. We have calculated gravity-wave production from the collision of two scalar-field vacuum bubbles, and, using an approximation based upon these results, from the collision of 20 to 30 vacuum bubbles. We present estimates of the relic background of gravitational waves produced by a first-order phase transition; in general, $\Omega_{GW} \sim 10^{-9}$ and $f \sim (10^{-6}\text{ Hz})(T/1\text{ GeV})$.

Crossover: beyond-SM physics:
axion-driven turbulence, Miniati et al. 2018

First order phase transitions?

gravitational waves primordial turbulence?

$$\nabla^2 \delta\rho(\boldsymbol{x},t) - \frac{1}{c_S^2}\frac{\partial^2}{\partial t^2}\delta\rho(\boldsymbol{x},t) = -\frac{\partial^2}{\partial x_i \partial x_j} T^{ij}(\boldsymbol{x},t) \qquad c_S^2 = \frac{\delta p}{\delta\rho}$$

$$\nabla^2 h_{ij}(\boldsymbol{x},t) - \frac{\partial^2}{\partial t^2} h_{ij}(\boldsymbol{x},t) = -16\pi G\, S_{ij}(\boldsymbol{x},t) \qquad c = 1$$

Aero-acoustic approximation:

- ✓ sound waves generation by turbulence
- ✓ Gravitational waves generation

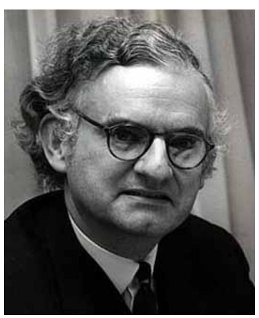

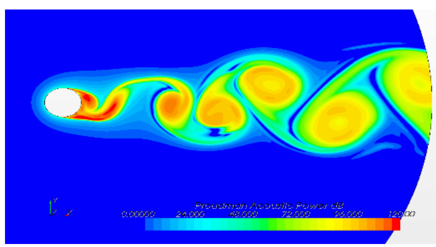

Lighthill, 1952; Proudman 1952

Kosowsky, Mack, Kahniashvili, 2002
Dolgov, Grasso, Nicolis, 2002
Gogoberidze, Kahniashvili, Kosowsky, 2002

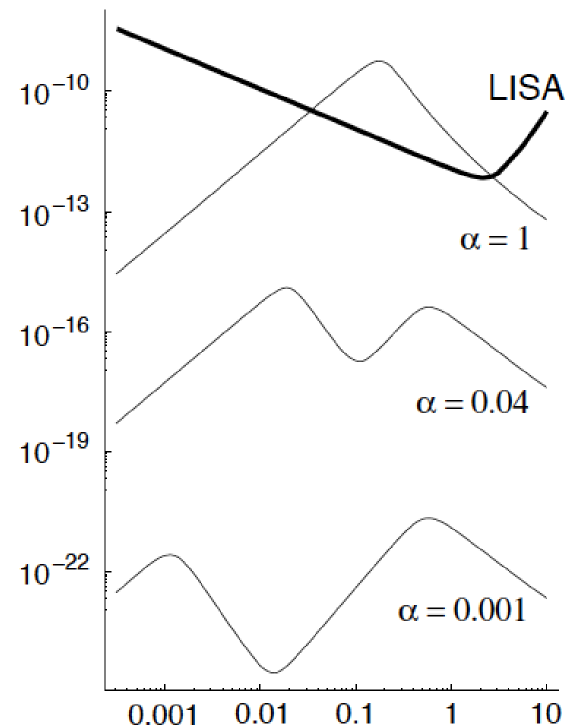

Nicolis 2004

why primordial turbulence?

Bubble nucleations

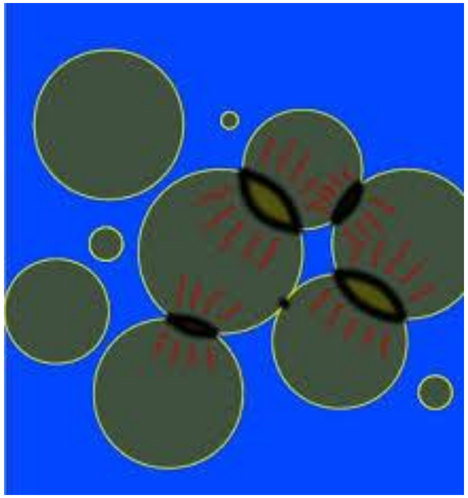

Baym et al. 1995

Magnetic fields

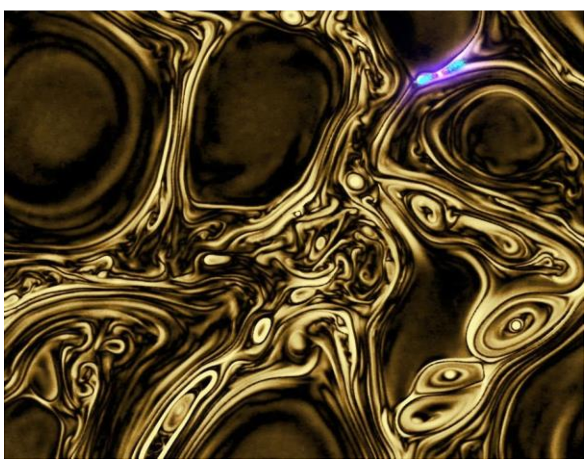

Quashnock, et al. 1989

- ✓ Injection of the magnetic energy at a given scale (phase transition bubble)
- ✓ Coupling of the magnetic field with primordial plasma

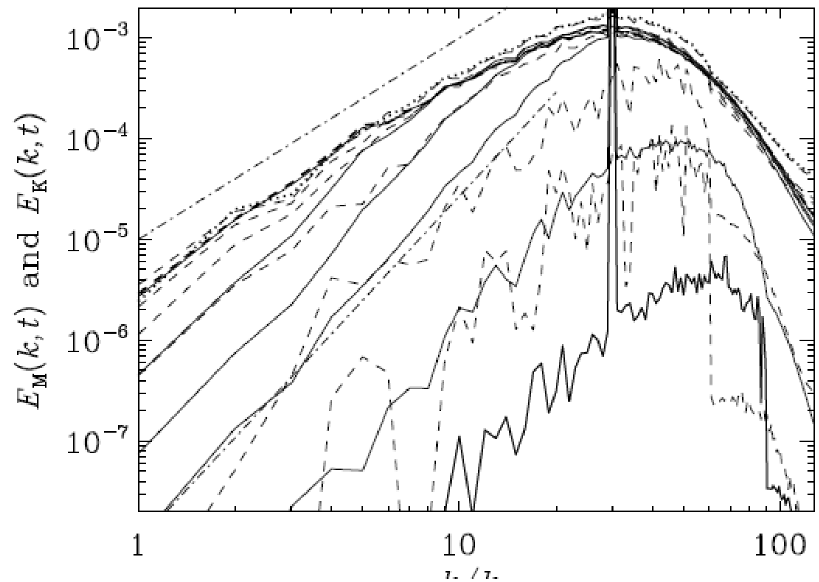

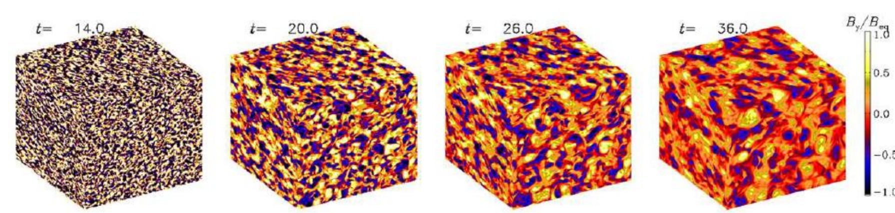

FIG. 2: Evolution of the turbulent magnetic field after turning off the forcing at time $t = 14\,t_1$. The B_y component is shown on the periphery of the computational domain.

Kahniashvili, et al. 2010

why primordial magnetic fields?

E Astrophysical Journal Letters, 727:L4 (4pp), 2011 January 20
doi:10.1088/2041-8205/727/1/L4

LOWER LIMIT ON THE STRENGTH AND FILLING FACTOR OF EXTRAGALACTIC MAGNETIC FIELDS

K. Dolag[1,2], M. Kachelriess[3], S. Ostapchenko[3,4], and R. Tomàs[5]
[1] Universitätssternwarte München, München, Germany
[2] Max-Planck-Institut für Astrophysik, Garching, Germany
[3] Institutt for fysikk, NTNU, Trondheim, Norway
[4] D. V. Skobeltsyn Institute of Nuclear Physics, Moscow State University, Moscow, Russia
[5] II. Institut für Theoretische Physik, Universität Hamburg, Germany
Received 2010 September 16; accepted 2010 November 25; published 2010 December 21

ABSTRACT

High-energy photons from blazars can initiate electromagnetic pair cascades interacting with the extragalactic photon background. The charged component of such cascades is deflected and delayed by extragalactic magnetic fields (EGMFs), thereby reducing the observed point-like flux and potentially leading to multi-degree images in the GeV energy range. We calculate the fluence of 1ES 0229+200 as seen by *Fermi*-LAT for different EGMF profiles using a Monte Carlo simulation for the cascade development. The non-observation of 1ES 0229+200 by *Fermi*-LAT suggests that the EGMF fills at least 60% of space with fields stronger than $\mathcal{O}(10^{-16}$ to $10^{-15})$ G for lifetimes of TeV activity of $\mathcal{O}(10^2$ to $10^4)$ yr. Thus, the (non-)observation of GeV extensions around TeV blazars probes the EGMF in voids and puts strong constraints on the origin of EGMFs: either EGMFs were generated in a space filling manner (e.g., primordially) or EGMFs produced locally (e.g., by galaxies) have to be efficiently transported to fill a significant volume fraction as, e.g., by galactic outflows.

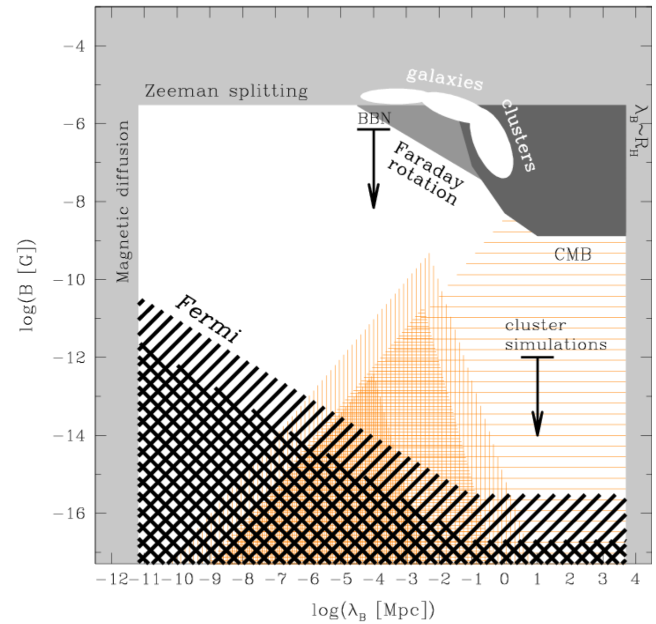

Neronov and Vovk 2010

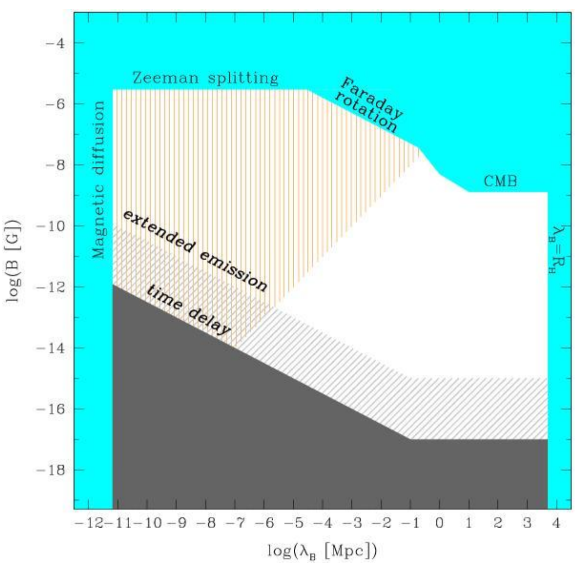

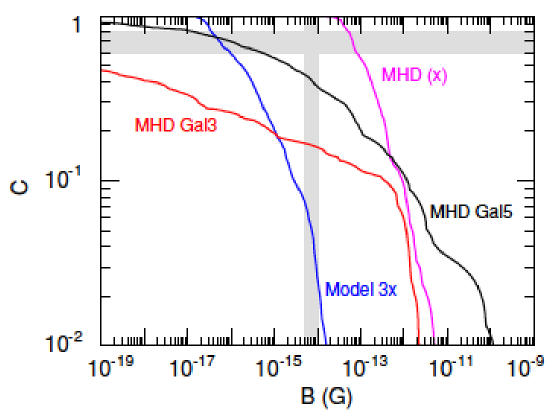

Figure 4. Cumulative volume filling factor $C(B)$ for the four different EGMF models found in MHD simulations.
(A color version of this figure is available in the online journal.)

4. SUMMARY

We have calculated the fluence of 1ES 0229+200 as seen by *Fermi*-LAT using a Monte Carlo simulation for the cascade development. We have discussed the effect of different EGMF profiles on the resulting suppression of the point-like flux seen by *Fermi*-LAT. Since the electron cooling length is much smaller than the mean free path of the TeV photons, a sufficient suppression of the point-like flux requires that the EGMF fills a large fraction along the line of sight toward 1ES 0229+200, $f \gtrsim 0.6$. The lower limit on the magnetic field strength in this volume is $B \sim \mathcal{O}(10^{-15})$ G, assuming 1ES 0229+200 is stable at least for 10^4 yr, weakening by a factor of 10 for $\tau = 10^2$ yr. These limits put very stringent constraints on the origin of EGMFs. Either the seeds for EGMFs have to be produced by a volume filling process (e.g., primordial) or very efficient transport processes have to be present which redistribute magnetic fields that were generated locally (e.g., in galaxies) into filaments and voids with a significant volume filling factor.

different magnetogenesis probes

- Gravitational waves propagate almost freely and retain the information about the source and physical processes
  - Frequency determines the source characteristic length scale
  - Amplitudes – the source efficiency and energetics.

$$f_{GW} = 2/l_S$$

$$N_b = \frac{H^{-1}}{l_S}$$

$$\Omega_{GW} \sim \Omega_B^2$$

$$\mathcal{E}_{\mathrm{GW}}(t) = \frac{1}{32\pi G} \langle \dot{h}^{\mathrm{TT}}_{ij,\mathrm{phys}}(\mathbf{x},t) \dot{h}^{\mathrm{TT}}_{ij,\mathrm{phys}}(\mathbf{x},t) \rangle$$

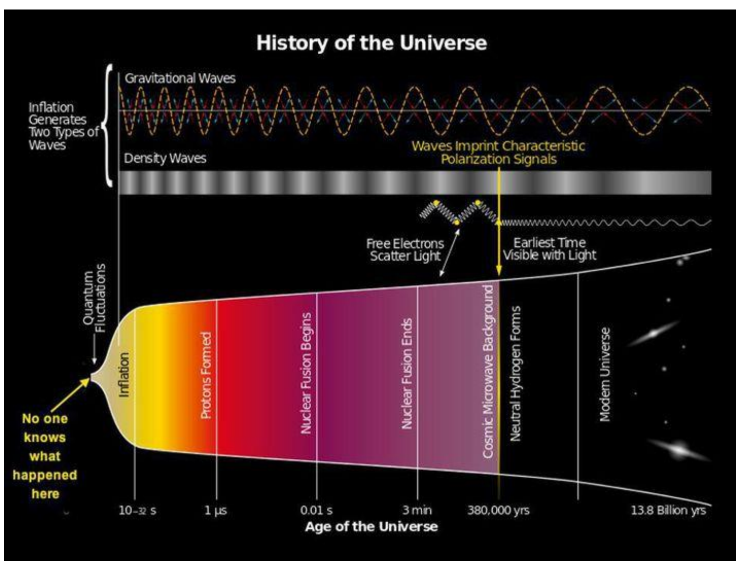

magnetic fields at recombination

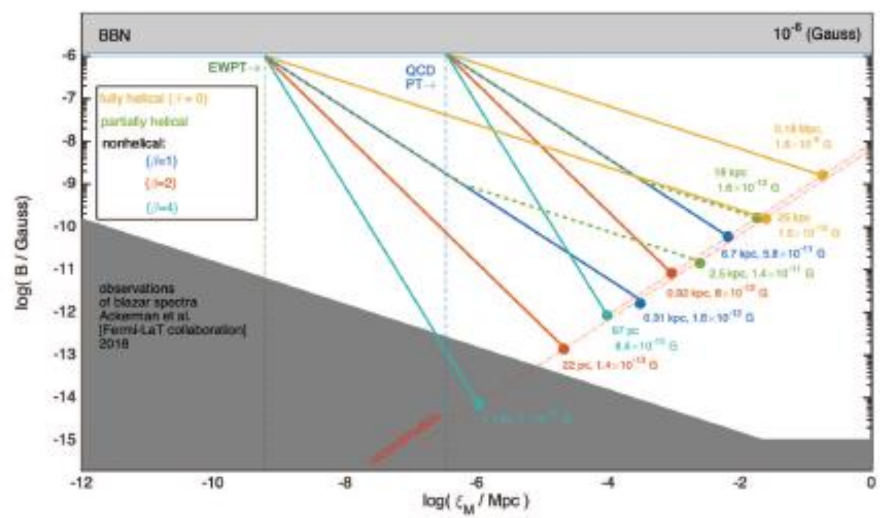

Credit: Emma Clarke

NANOGrav 12.5 years observations:

NANOGrav 12.5-year sensitivity range of 1–100 nHz

$$h_c(f) = A_{\mathrm{CP}} \left(\frac{f}{f_{\mathrm{yr}}} \right)^{\alpha_{\mathrm{CP}}},$$

$$\Omega_{\mathrm{GW}}(f) = \frac{2\pi^2}{3H_0^2} f^2 h_c^2(f) = \Omega_{\mathrm{GW}}^{\mathrm{yr}} \left(\frac{f}{f_{\mathrm{yr}}} \right)^{5-\gamma_{\mathrm{CP}}}$$

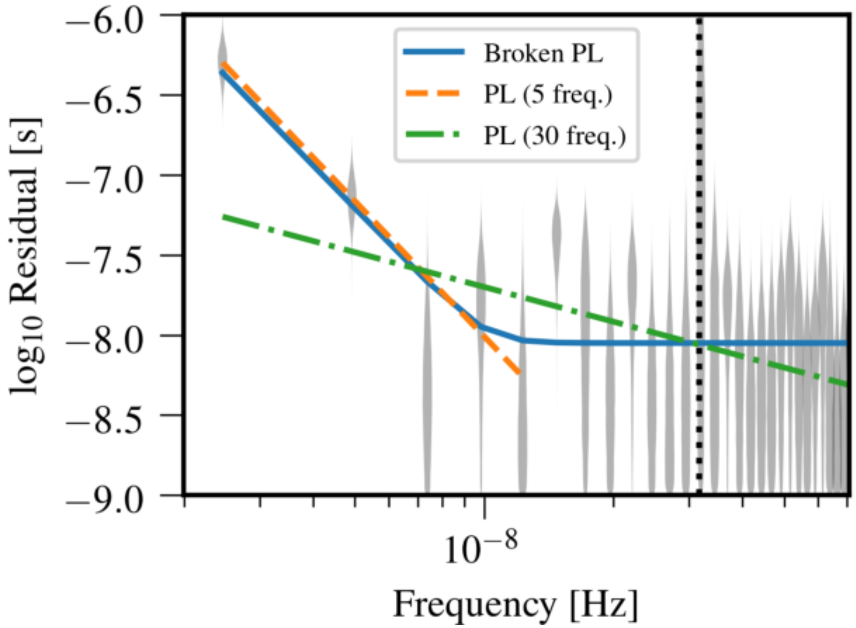

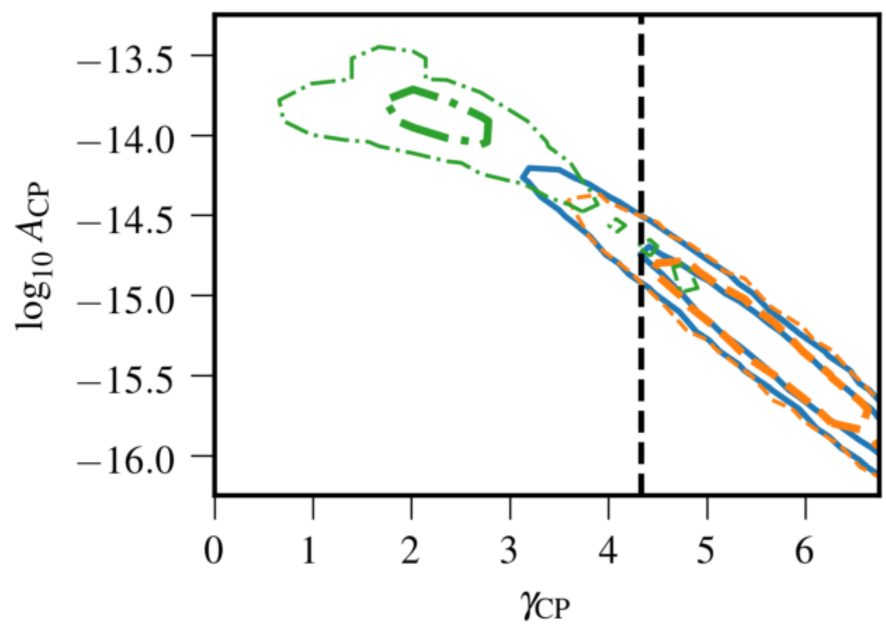

$$\Omega_{\mathrm{GW}}(t, f) = \frac{1}{\mathcal{E}_{\mathrm{crit}}(t)} \frac{\mathrm{d}\mathcal{E}_{\mathrm{GW}}}{\mathrm{d}\ln f}$$

Arzoumanian et al (2021)

Possible Sources:

Astrophysical:

✓ Super massive black hole binary (SMBHB) (Phinney 2001): γ=13/3

Cosmological:

✓ Bubbles collisions (Kosowsky et. Al. 1993)
✓ Inflation (Vagnozzi 2021)
✓ Cosmic strings (Blanco-Pillado et al. 2021)
✓ Seed magnetic fields (Neronov et. al. 2021)
✓ Hydrodynamic and MHD Turbulence (Brandenburg et al. 2021)

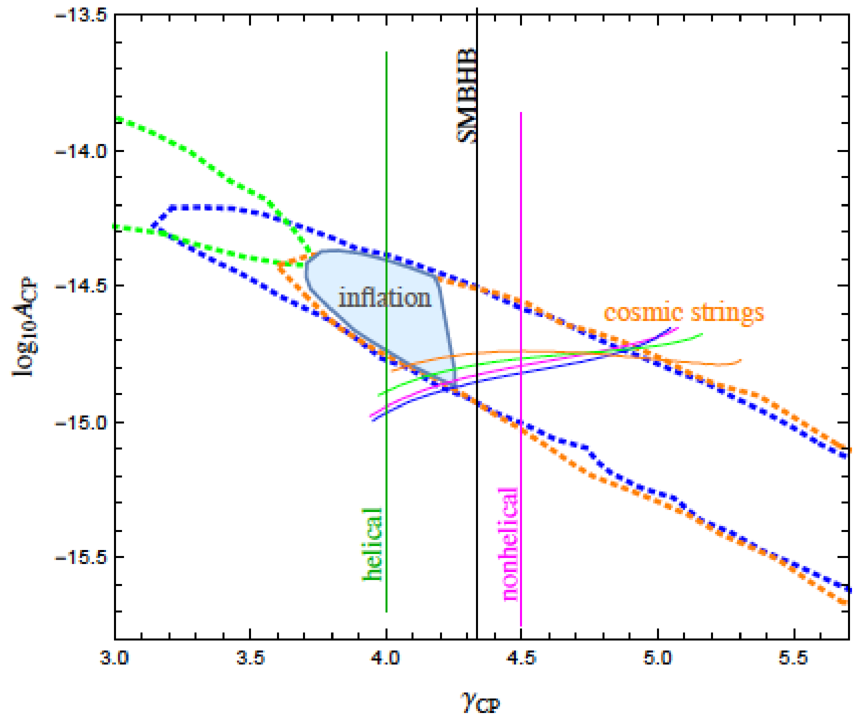

Credit: Emma Clarke

QCD energy scale

$$\frac{a_0}{a_\star} = 10^{12}\left(\frac{g_{S,\star}}{15}\right)^{\frac{1}{3}}\left(\frac{T_\star}{150\ \mathrm{MeV}}\right)$$

$$H_\star^2 = \frac{8\pi G}{2}\mathcal{E}_{\mathrm{rad},\star} \qquad \mathcal{E}_{\mathrm{rad},\star} = \frac{\pi^2 g_\star}{30}T_\star^4 \qquad (c = k_B = \hbar = 1)$$

$$f_H \simeq (1.8\times10^{-8}\mathrm{Hz})10^{12}\left(\frac{g_\star}{15}\right)^{\frac{1}{3}}\left(\frac{T_\star}{150\ \mathrm{MeV}}\right)$$

NANOGrav 12.5 years observations vs. QCD:

Arzoumanian et al (2021)

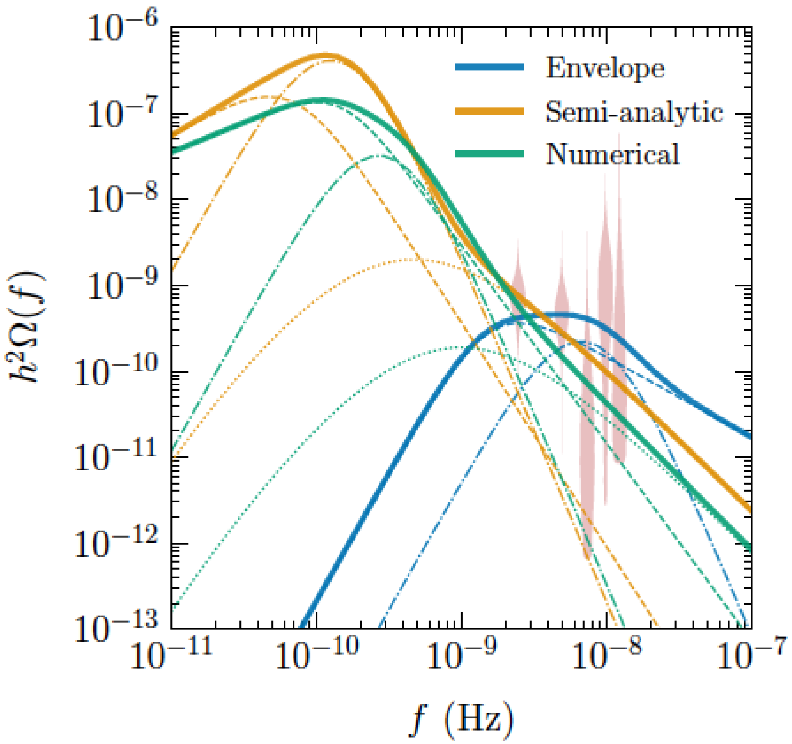

Maximum likelihood GWB fractional energy-density spectrum compared with the marginalized posterior for the free power. spectrum (independent per-frequency characterization; red violin plot). The blue, oranage, and green lines represent the maximum likelihood spectra derived using the envelope, semi-analytical, and numerical results for the bubble contribution. The breakdown of the spectrum is shown in the three contributions: bubble (dashed lines), sound waves (dash-doted lines), and turbulence (dotted lines).

The values of (α, T) for these maximum likelihood spectra are (2.3, 2.8 MeV) for the envelope results, (2.3, 1.7 MeV) for the semi-analytic results, and (2.1, 2.5 MeV) for the numerical result

- T the Universe temperature at which the phase transition takes place.
- α the strength of the phase transition, defined as the ratio of the vacuum and relativistic energy density at the time of the phase transition.
- β/H the bubble nucleation rate in units of the Hubble rate at the time of the phase transition

numerical simulations

$$\left(\frac{\partial^2}{\partial t^2} - c^2\nabla^2\right) h_{ij}^{\rm TT} = \frac{16\pi G}{a^3 c^2} T_{ij}^{\rm TT},$$

$$h_{ij}^{\rm TT} = a h_{ij}^{\rm TT,phys} \qquad {\rm d}t_{\rm phys} = a{\rm d}t$$

Grishchuk 1974

- ✓ To account properly non-linear processes (MHD)
- ✓ Not be limited by the short duration of the phase transitions
- ✓ Two stages turbulence decay
  - Forced turbulence
  - Free decay
- ✓ The source is present till recombination (after the field is frozen in)
- ✓ Results – strongly initial conditions dependent

$$\frac{\partial \ln\rho}{\partial t} = -\frac{4}{3}(\nabla\cdot u + u\cdot\nabla\ln\rho) + \frac{1}{\rho}\left[u\cdot(J\times B) + \eta J^2\right],$$

$$\frac{\partial u}{\partial t} = -u\cdot\nabla u + \frac{u}{3}(\nabla\cdot u + u\cdot\nabla\ln\rho) + \frac{2}{\rho}\nabla\cdot(\rho\nu\mathbf{S}) - \frac{1}{4}\nabla\ln\rho - \frac{u}{\rho}\left[u\cdot(J\times B) + \eta J^2\right] + \frac{3}{4\rho}J\times B,$$

$$\frac{\partial B}{\partial t} = \nabla\times(u\times B - \eta J + \mathcal{F}), \quad J = \nabla\times B.$$

$$\mathcal{E}_{\rm M}(t) = \mathcal{E}_{\rm M}^{\rm max}(1+\Delta t/\tau)^{-p} \qquad \mathcal{E}_{\rm GW}^{\rm sat} = (q\mathcal{E}_{\rm M}^{\rm max}/k_{\rm f})^2$$

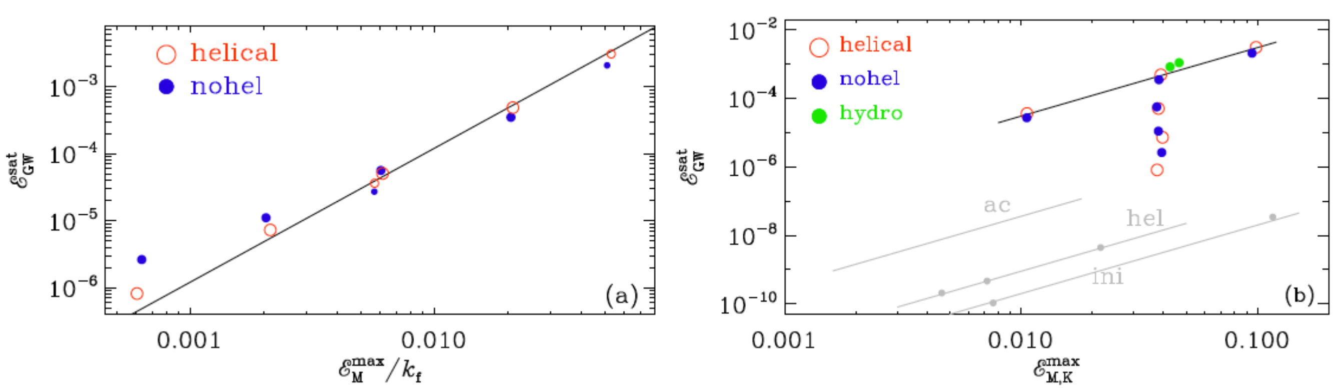

Brandenburg et al (2021) [arXiv:2102.12428]

Results

TABLE I: Summary of runs with nonhelical turbulence.

Run	k_f	k_1	f_0	p	τ	$\mathcal{E}_M^{max}$	$\mathcal{E}_{GW}^{sat}$	h_{rms}^{sat}	B [μG]	$h_0^2\Omega_{GW}(f)$	h_c
noh1	2	0.3	1.9×10^{-1}	1.0	16	3.83×10^{-2}	3.53×10^{-4}	4.83×10^{-2}	0.78	1.09×10^{-8}	4.83×10^{-14}
noh2	6	1	6.0×10^{-2}	1.0	4.5	3.75×10^{-2}	5.61×10^{-5}	7.06×10^{-3}	0.78	1.73×10^{-9}	7.07×10^{-15}
noh3	20	3	2.3×10^{-2}	1.3	2.0	3.81×10^{-2}	1.11×10^{-5}	1.15×10^{-3}	0.78	3.44×10^{-10}	1.15×10^{-15}
noh4	60	10	1.0×10^{-2}	1.4	0.43	3.93×10^{-2}	2.62×10^{-6}	1.65×10^{-4}	0.79	8.10×10^{-11}	1.65×10^{-16}
noh5	2	0.3	1.0×10^{-1}	—	—	1.06×10^{-2}	2.70×10^{-5}	1.40×10^{-2}	0.41	8.37×10^{-10}	1.40×10^{-14}
noh6	2	0.3	3.0×10^{-1}	—	—	9.48×10^{-2}	2.08×10^{-3}	1.02×10^{-1}	1.2	6.42×10^{-8}	1.02×10^{-13}
noh7	6	1	2.0×10^{-2}	—	—	4.63×10^{-3}	6.56×10^{-7}	8.10×10^{-4}	0.27	2.03×10^{-11}	8.11×10^{-16}
noh8	6	1	1.0×10^{-1}	—	—	8.90×10^{-2}	3.89×10^{-4}	1.67×10^{-2}	1.2	1.20×10^{-8}	1.67×10^{-14}

TABLE II: Similar to Table I, but for helical turbulence.

Run	k_f	k_1	f_0	p	τ	$\mathcal{E}_M^{max}$	$\mathcal{E}_{GW}^{sat}$	h_{rms}^{sat}	B [μG]	$h_0^2\Omega_{GW}(f)$	h_c
hel1	2	0.3	1.9×10^{-1}	0.67	100	3.90×10^{-2}	4.85×10^{-4}	4.33×10^{-2}	0.79	1.50×10^{-8}	4.33×10^{-14}
hel2	6	1	5.6×10^{-2}	0.67	20	3.81×10^{-2}	5.05×10^{-5}	4.69×10^{-3}	0.78	1.56×10^{-9}	4.69×10^{-15}
hel3	20	3	2.0×10^{-2}	0.67	4.0	3.96×10^{-2}	7.26×10^{-6}	6.66×10^{-4}	0.80	2.24×10^{-10}	6.66×10^{-16}
hel4	60	10	6.5×10^{-3}	0.67	0.50	3.76×10^{-2}	8.15×10^{-7}	7.18×10^{-5}	0.78	2.52×10^{-11}	7.18×10^{-17}
hel5	2	0.3	1.0×10^{-1}	—	—	1.06×10^{-2}	3.61×10^{-5}	1.08×10^{-2}	0.41	1.12×10^{-9}	1.08×10^{-14}
hel6	2	0.3	3.0×10^{-1}	—	—	9.85×10^{-2}	3.07×10^{-3}	1.12×10^{-1}	1.3	9.49×10^{-8}	1.12×10^{-13}
hel7	6	1	2.0×10^{-2}	—	—	4.93×10^{-3}	8.33×10^{-7}	6.26×10^{-4}	0.28	2.58×10^{-11}	6.26×10^{-16}
hel8	6	1	1.0×10^{-1}	—	—	1.20×10^{-1}	5.09×10^{-4}	1.59×10^{-2}	1.4	1.57×10^{-8}	1.59×10^{-14}

Brandenburg et al (2021)
[arXiv:2102.12428]

Results

$$\mathcal{E}_{\rm M}(t) = \mathcal{E}_{\rm M}^{\rm max}\,(1 + \Delta t/\tau)^{-p}$$

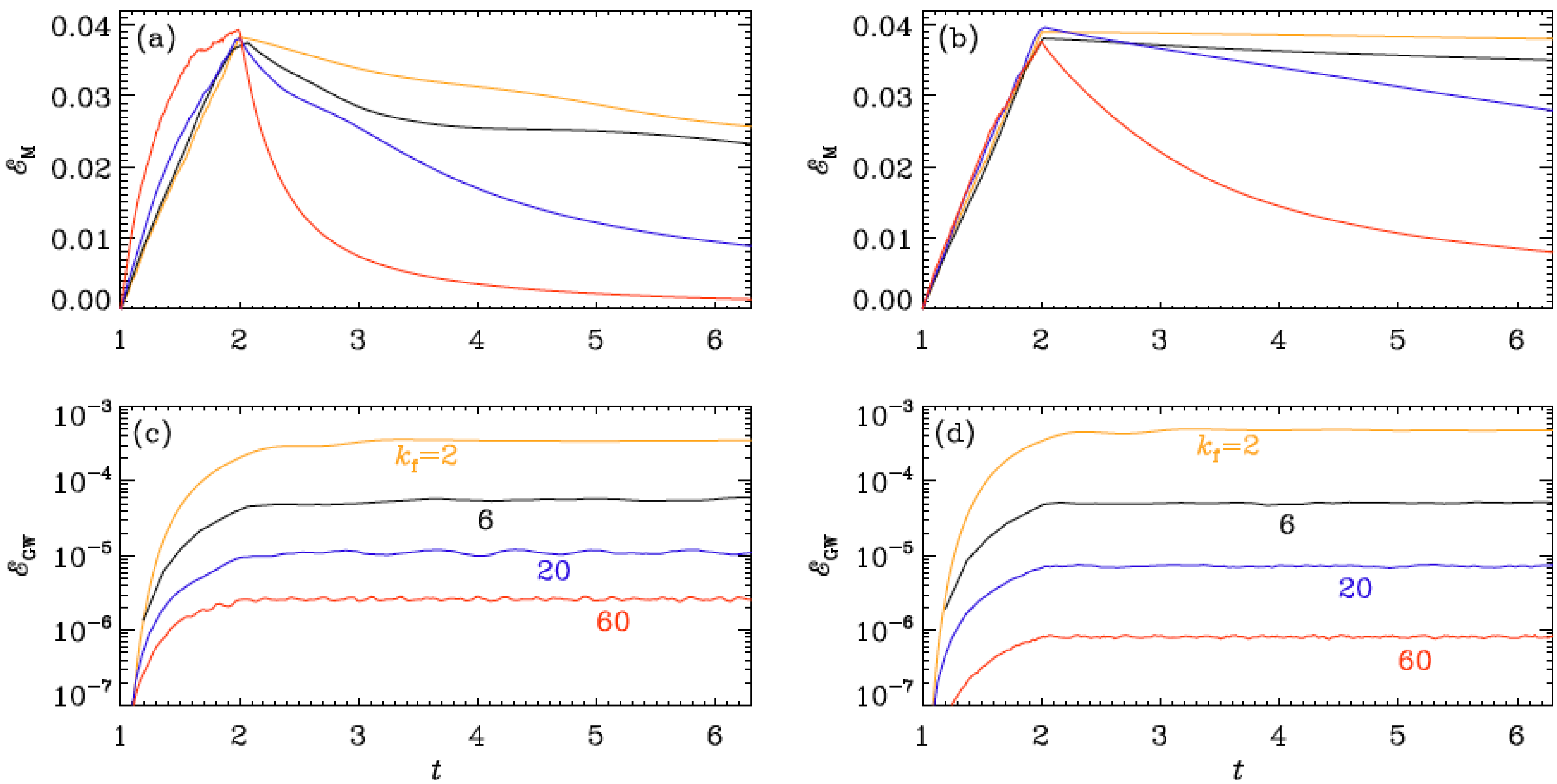

Evolution of $E_M(t)$ and $E_{GW}(t)$ for nonhelical (left) and helical (right) cases. Orange, black, blue, and red are for k_f = 2, 6, 20, and 60, respectively.

Brandenburg et al (2021)
[arXiv:2102.12428]

Results

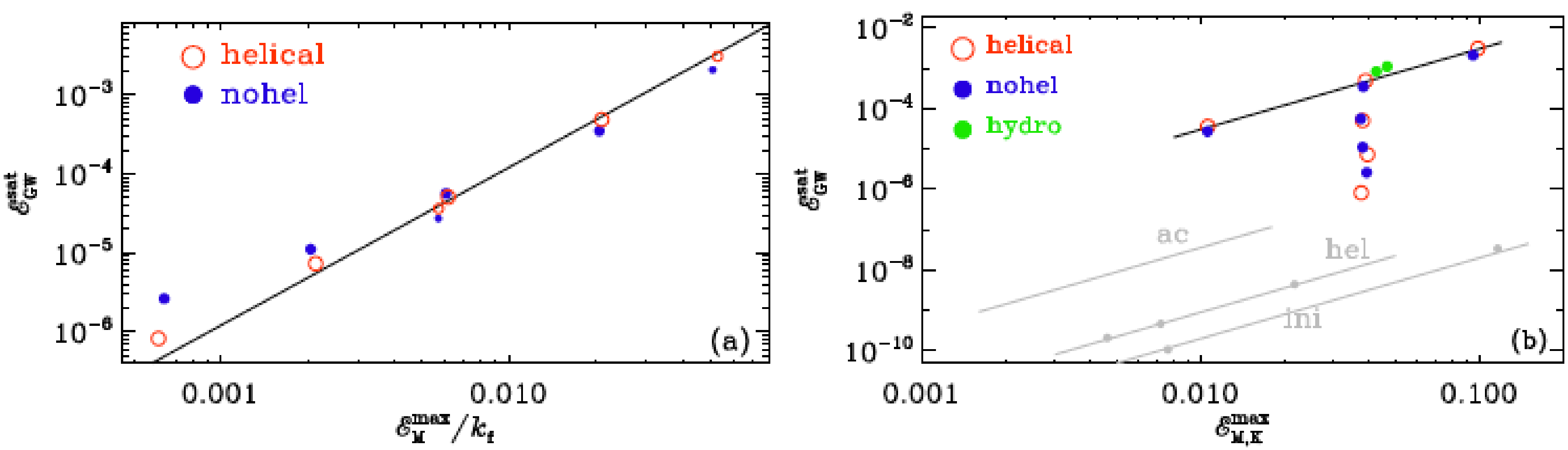

FIG. 4: (a) $\mathcal{E}_{\rm GW}$ versus $\mathcal{E}_{\rm M}/k_{\rm f}$; the straight line shows $\mathcal{E}_{\rm GW} = 5.2 \times 10^{-4}\,(\mathcal{E}_{\rm M}/k_{\rm f})^{1/2}$. (b) Positions of our runs in a diagram showing $\mathcal{E}_{\rm GW}^{\rm sat}$ versus $\mathcal{E}_{\rm M}^{\rm max}$. For orientation the old data points of the Ref. [73] are shown as gray symbols. The open red (filled blue) symbols are for the helical (nonhelical) runs. The green symbols refer to the two hydromagnetic runs of Table III.

TABLE III: Comparison of nonhelical magnetic turbulence (mag) with irrotational (irro) and vortical (vort) turbulence.

Type	f_0	ν	$\mathcal{E}_{\rm M}^{\rm max}$	$\mathcal{E}_{\rm GW}^{\rm sat}$	$h_{\rm rms}^{\rm sat}$	B [μG]	$h_0^2\Omega_{\rm GW}(f)$	$h_{\rm c}$
magnetic	1.9×10^{-1}	5.0×10^{-5}	3.83×10^{-2}	3.53×10^{-4}	4.83×10^{-2}	0.78	1.09×10^{-8}	4.83×10^{-14}
vortical	3.8×10^{-1}	1.0×10^{-2}	4.21×10^{-2}	8.81×10^{-4}	8.26×10^{-2}	0.82	2.73×10^{-8}	8.27×10^{-14}
irrotational	7.0×10^{-1}	2.0×10^{-2}	4.26×10^{-2}	8.30×10^{-4}	7.95×10^{-2}	0.83	2.57×10^{-8}	7.96×10^{-14}

Brandenburg et al (2021)
[arXiv:2102.12428]

Results

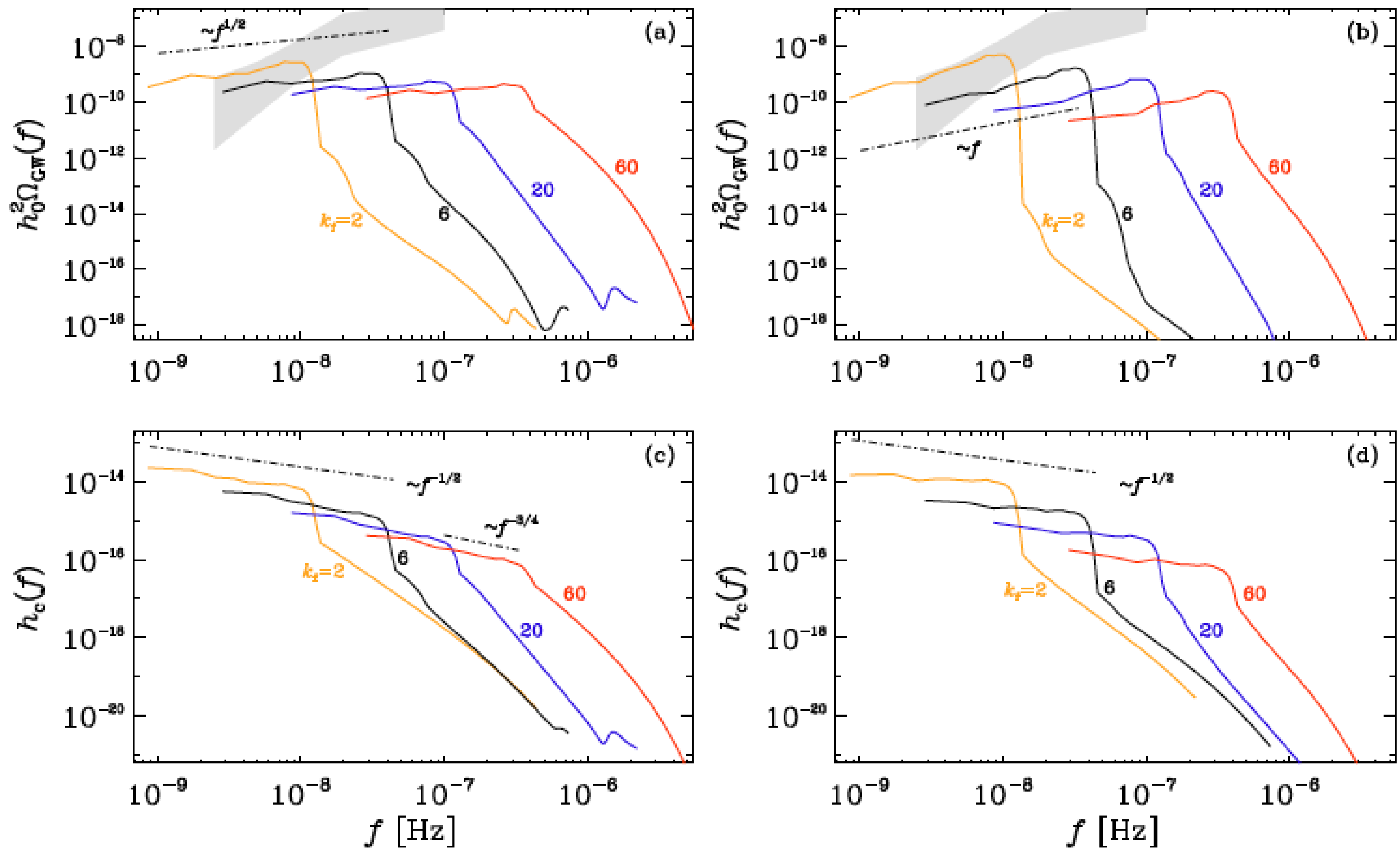

FIG. 5: $h_0^2\Omega_{GW}(f)$ and $h_c(f)$ at the present time for all four runs presented in Table I, for the nonhelical (left) and helical (right) runs. The 2σ confidence contour for the 30-frequency power law of the NANOGrav 12.5-year data set is shown in gray.

Brandenburg et al (2021) [arXiv:2102.12428]

Results

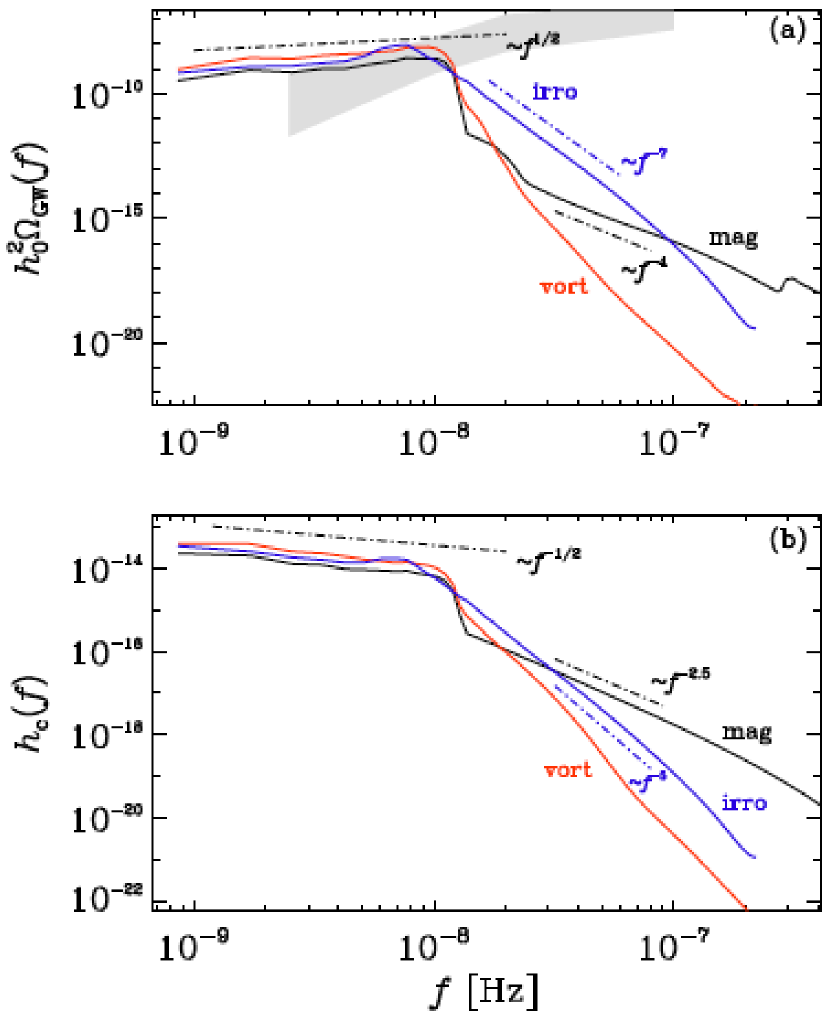

FIG. 7: Similar to Fig. 5, but comparing vortical (red) and irrotational turbulence (blue) with MHD turbulence (black).

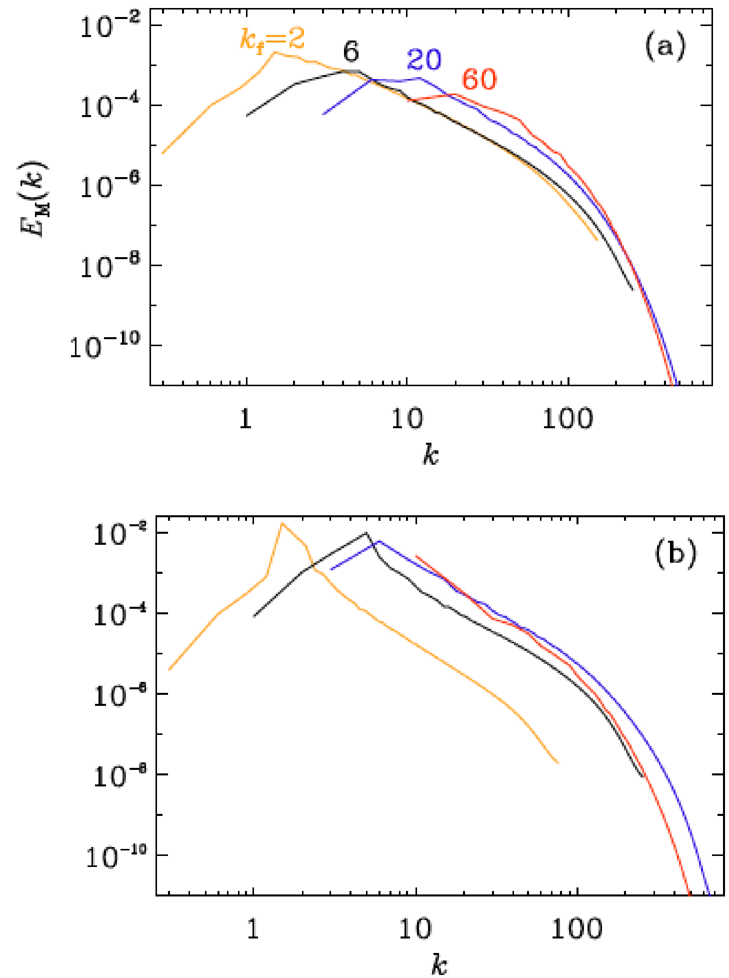

Magnetic energy spectra for the (a) nonhelical and (b) helical cases

Brandenburg et al (2021) [arXiv:2102.12428]

Conclusions

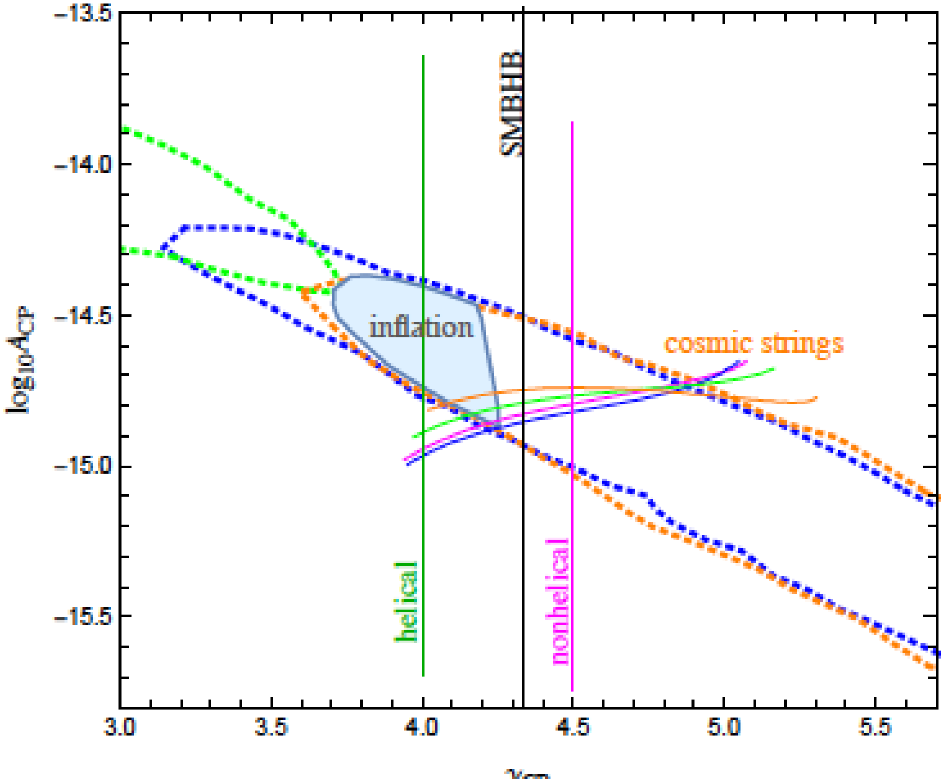

Hydrodynamic and MHD Turbulence @ QCD scale (this work):

- $f < f_{\rm peak}$: $\gamma \approx 4$ (helical), $\gamma \approx 4.5$ (non-helical)
- $f > f_{\rm peak}$: $\gamma \approx 12$ (kinetic), $\gamma \approx 9$ (mhd)

Credit: Emma Clarke

✓ *Magnetic stress from hydrodynamic and MHD turbulence with scales comparable to the cosmological horizon scale at the QCD transition can drive GWs in the range accessible to NANOGrav if the magnetic energy density is 3-10% of the radiation energy density.*

✓ *Our work's new insights regarding the possibility of using an observed GW spectrum for making statements about the nature of the underlying turbulence in the early universe. One is the already mentioned slope of the subinertial range spectrum. Another is the position of the peak of the spectrum*

✓ *The specific features of the spectrum near the peak are different for helical and nonhelical turbulence. This could, in principle, give information about the presence of parity violation, when would also lead to circularly polarized GWs.*

Next steps

Determine the mechanisms insuring the presence of viable turbulent sources and correspondingly correct initial conditions:

- ❖ Primordial magnetogenesis
- ❖ Bubble collisions/nucleation – more realistic models
- ❖ Sound waves as a source for turbulence
- ❖ Axions driven turbulence and axion like particles driven inflationary new physics
- ❖ Low temperature re and pre-heating

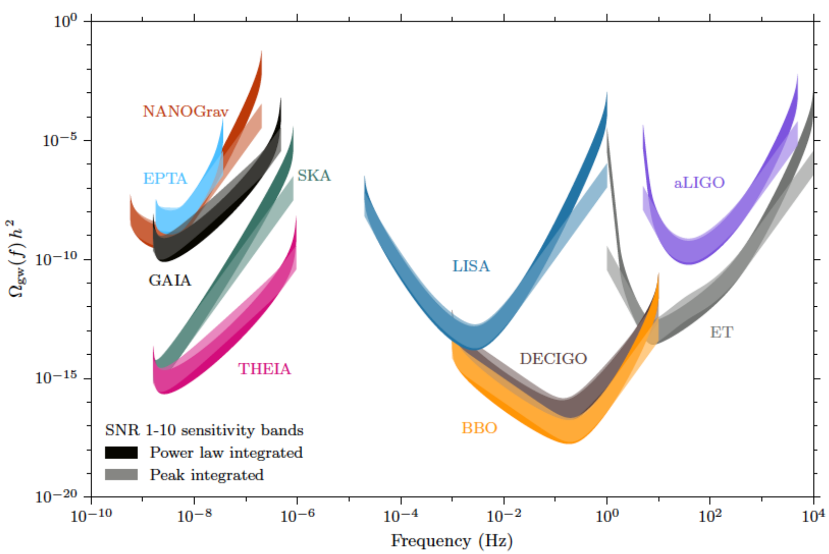

Cross-correlating data between different observations:

- ❖ PTAs
- ❖ Astrometric missions: Gaia, Theia

$$\Omega_{\rm gw}(f)\,h^2 = \frac{2\pi^2}{3H_0^2} f^2 h_{\rm gw}^2(f) h^2$$

Garcia-Bellido et al. 2021
arXiv: 2104.04778

Thank you!

To Organizers

To Co-Authors and Collaborators (on related subjects):

- Axel Brandenburg
- Emma Clarke
- Grigol Gogoberidze
- Yutong He
- Arthur Kosowsky
- Andrew Long
- Sayan Mandal
- Alberto Roper Pol
- Jeniffer Schober
- Nakul Shenoy
- Jonathan Stepp

To Audience